

Strong-Weak Bi-Adjoint, Gluon-W resonances, and new asymmetric LHC production processes

Linda M. Carpenter¹ and Katherine Schwind¹

¹*Department of Physics, The Ohio State University and Center for Cosmology and AstroParticle Physics*

We study a novel production and decay mechanism for a bi-adjoint spin zero particle in the (8,3,0) representation of the Standard Model gauge groups. This work is part of a series studying new production processes for exotic particles in higher representations of Standard Model color and weak charge. We study a new dimension 5 effective operator model which couples an exotic bi-adjoint scalar field to the SU(3) and SU(2) field strength tensors. We explore the W-gluon resonant decay of the charged component of this new exotic field. We discuss LHC production modes of the charged and neutral bi-adjoint state and find a new single production mode for the charged state that is the dominant LHC production mode for TeV-scale masses. We introduce a new HL-LHC search in this asymmetric W-gluon fusion process in which a single bi-adjoint is produced in association with a hard forward quark jet. We have 5 sigma discovery potential for bi-adjoint masses up to 3 TeV for 10 TeV scalar effective operator cutoffs. We also find 2 sigma sensitivity of HL-LHC for bi-adjoint masses up to 4 TeV and effective cut-offs in the 15 TeV range for the full 3 inverse atto-barn data set.

I. INTRODUCTION

This work is part of a series exploring new Light Exotic (LEX) particles that couple to the Standard Model through effective operators. In this series we catalog under-explored and uncharted phenomenology for exotic particles with unusual Standard Model charges [1–6]. Since we do not know what new physics the universe might have in store for us, general EFT model building techniques allow us to survey a broad landscape of potential new interactions. Among the models with the most compelling phenomenology that have remained understudied are those with exotic states that carry both large SU(3) and SU(2) charges. It is this type of signature that the current paper will address. BSM scenarios with exotic particles charged under SU(3) tend to be studied under the assumption they are singlets under SU(2). Some of the most well-known exotics models of this type include neutral scalar color octet scalars, neutral fermionic color octets like gluinos, and SU(2) singlet color sextets [2–4, 7–9]. Colored particles with SU(2) representations that are fundamental and higher have received less attention with the noted exception of left-handed squarks and Manohar-Wise weak doublet color octets [10]. Both of these last examples are SU(2) doublets, the lowest non-trivial representation of SU(2). Here, we propose studying exotics in higher dimensional representations of SU(3) and SU(2) which might have unusual effective couplings to Standard Model fields.

In this work, we study a scalar field in the adjoint representations of both the SU(3) and SU(2) gauge groups. The field we study has zero hypercharge, and we thus denote this "bi-adjoint" as being in the (8,3,0) representation of the Standard Model (SM) gauge groups.

Studies of exotic color octets usually focus on models in low-dimensional representations of SU(2). Many phenomenological studies have been made on neutral color octets in the (8,1,0) representation of SM gauge groups [9, 11–16]. Less phenomenological attention has fallen on the Manohar-Wise model, involving an SU(2) doublet color octet in the (8,2,1) representation of the SM, but several efforts have been made to explore the phenomenological parameter space [17–19]. The Manohar-Wise field may couple directly to pairs of quarks at tree level. Both the (8,1,0) and (8,2,1) exotic octets have the feature that their neutral components can be singly produced through gluon fusion. As such, this is a primary feature of their collider phenomenology and di-jet resonance is an important discovery signature. The (8,3,0) bi-adjoint is interesting as it has no renormalizable couplings to quarks and further, the bi-adjoint single production through gluon fusion occurs only at dimension 7 in effective field theory, through an operator suppressed by a scale v^2/Λ^3 . Since the di-gluon and di-quark couplings of the bi-adjoint are suppressed, the main phenomenological signatures of the bi-adjoint model are varied and quite a bit different from other color octet models.

Effective operators at dimension 5 are important to color octet models. Indeed, it is a dimension 5 operator which generates the coupling to two gluons that allows gluon fusion single production of color octets in the (8,1,0) and (8,2,1) models. The bi-adjoint couples to the Standard Model through the dimension 5 effective operator

$$\frac{1}{\Lambda} \phi W^{\mu\nu} G_{\mu\nu} \quad (1)$$

This operator was first discussed in references [6],[1] and [5] which cataloged new types of exotic states that could

be reached through the W-gluon portal. The W-gluon portal is an unusual sector of the di-boson portal, the region of theory space where exotic particles couple to the SM through pairs of SM gauge bosons.

This new interaction contains interesting couplings between the charged component of ϕ and a W-gluon pair of gauge bosons. The operator opens a host of new and unusual collider production modes for the bi-adjoint. This includes a new W-gluon resonant decay mode of the charged components of the bi-adjoint, and Z-gluon/Z-photon decays of the neutral component. In this work we explore the mass spectrum of the bi-adjoint model and the unusual di-boson couplings of the bi-adjoint states. We discuss new single production modes for the charged and neutral bi-adjoints that result from the dimension 5 operator, focusing on production modes that follow from the W-gluon coupling. We introduce a new asymmetric LHC production mode for ϕ single production involving an asymmetric W-gluon fusion process where a gluon fuses with W, which radiates off of an incoming quark, and a single ϕ is produced in association with a hard forward jet. We create a new HL-LHC sensitivity analysis and find that we have 5 σ discover potential for ϕ masses in the multi-TeV range for cutoffs over 10 TeV. We also have 2 σ sensitivity to multi-TeV scalars with cutoff up to 20 TeV.

This paper proceeds as follows. In Section 2 we introduce the model. In Section 3 we discuss decays of the bi-adjoints. In section 4 we discuss LHC production modes. In Section 5 we propose a new search for charged bi-adjoints and perform an HL-LHC sensitivity analysis. Section 6 concludes.

II. MODEL

With this model we consider the couplings of a spin-0 scalar in the (8,3,0) representations of the SU(3), SU(2), and U(1) gauge groups. We refer to this state as the "bi-adjoint" as it is in the adjoint representations of both the SU(3) and SU(2) gauge groups. This is thus a model of an exotic color octet with higher SU(2) charge. We will start by exploring the Lagrangian.

First, note that the bi-adjoint has components with charge +1, 0, -1. The adjoint may be expressed in the real representation, written in 2×2 matrix form as

$$\phi = \begin{pmatrix} \phi_0/\sqrt{2} & \phi^+ \\ \phi^- & -\phi^0/\sqrt{2} \end{pmatrix}. \quad (2)$$

The new field has standard kinetic terms. Writing this with the most general tree-level mass terms and dimension 4 Higgs interaction terms we have

$$L_{0R} = |D_\mu \phi|^2 + M^2 Tr[\phi\phi] + y|H_k|^2 Tr(\phi\phi) + \delta\phi^3 + \text{quartics}. \quad (3)$$

In the above Lagrangian ϕ is the (8,3,0) bi-adjoint field and H is the Standard Model Higgs field. Lower case letters indicate SU(2) fundamental indices. The parameter M is a standard mass shared by all of the components of ϕ . For this real representation there is only one independent Higgs coupling term. Both this term and the mass term couple to $Tr[\phi\phi]$. In the real representation, the masses of the charged and neutral states are not split by the Higgs interaction and all states in the multiplet are degenerate. There is an allowed tri-linear coupling of the bi-adjoint proportional to a parameter we call δ which has dimensions of mass. The quartic terms involving the bi-adjoints are enumerated in the appendix.

Instead, let ϕ be a complex field, with real and imaginary components $\phi = \phi_R + i\phi_I$. Counting real and imaginary states of different charges, there are six total components of ϕ . The Lagrangian is considerably more complicated than the real model.

$$L_{0C} = |D_\mu \phi|^2 + m^2 \phi\phi^\dagger + \frac{1}{2} M^2 Tr[\phi\phi] + \frac{1}{2} \lambda_1 |H_k|^2 Tr(\phi\phi) + \lambda_2 |H_k|^2 \phi\phi^\dagger \\ + \lambda_3 (H^{\dagger k} \phi_k^j)(\phi_j^{i\dagger} H_i) + \lambda_4 (H^{\dagger k} \phi_k^{\dagger j})(\phi_j^i H_i) + \lambda_5 (H^{\dagger k} \phi_k^j)(\phi_j^i H_i) + \delta\phi^3 + \delta_2 \phi|\phi|^2 + \text{quartics} + h.c. \quad (4)$$

This Lagrangian is similar to the Lagrangian for a Higgs triplet field [20–23] and to the scalar potential of supersymmetric theories with pure SU(2) adjoints [24–26]. However, differs in some key features such that we have to take care with CP conservation. For complex bi-adjoint fields, there is a possible mass term m_2 involving $\phi\phi^\dagger$ and a second type of mass term M^2 involving $\phi\phi$ plus its hermitian conjugate. This type of mass is not allowed in triplet Higgs models due to hypercharge conservation. The mass parameter M splits the masses of the real and imaginary components of ϕ . There are several new possible Higgs interactions allowed by all symmetries. The parameter λ_1

further splits the masses of the real and imaginary states. When Higgs vevs are inserted λ_2 provides a mass term similar to m^2 . After insertion of Higgs vevs, the λ_3 and λ_4 terms split the masses between the differently charged states. This splitting has an analog from a similar operator in the Higgs triplet model. The neutral mass eigenstates are

$$m_{\phi_R}^2 = (m^2 + (\lambda_1 + \lambda_2)v^2 + M^2 + \lambda_5 v^2 + \lambda_3 \frac{v^2}{2} + \lambda_4 \frac{v^2}{2}) \quad (5)$$

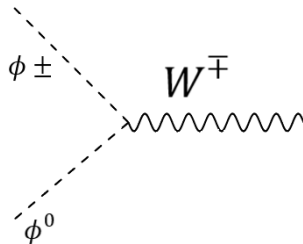
$$m_{\phi_I}^2 = (m^2 + (-\lambda_1 + \lambda_2)v^2 - M^2 - \lambda_5 v^2 + \lambda_3 \frac{v^2}{2} + \lambda_4 \frac{v^2}{2}) \quad (6)$$

To compute the masses of charged states we must diagonalize the mass matrix

$$\begin{array}{cc} & \begin{array}{c} \phi^+ \\ \phi^{-\dagger} \end{array} \\ \begin{array}{c} \phi^{+\dagger} \\ \phi^- \end{array} & \begin{pmatrix} m^2 + \lambda_2 v^2 + \lambda_3 v^2 & M^2 + \lambda_1 v^2 + \lambda_5 v^2 \\ M^2 + \lambda_1 v^2 + \lambda_5 v^2 & m^2 + \lambda_2 v^2 + \lambda_4 v^2 \end{pmatrix} \end{array}$$

For the mass eigenstates of the charged states to be pure real or imaginary ϕ components, the off diagonal parameters M and $\lambda_{1,5}$ must be zero if $\lambda_3 \neq \lambda_4$.

The kinetic term contains the coupling of the ϕ components to SU(2) and SU(3) gauge bosons. Particularly important is the interaction which couples the charged and neutral components of the ϕ field to a W boson as pictured below. These interactions allow either the charged or neutral component of ϕ to decay to an on or off-shell W boson and the lighter component if the mass splitting parameter is non-zero.



However, we note that at this level with L_0 couplings only, the lightest bi-adjoint mode is stable at tree level. We must assume further interactions for the lightest state to decay. Both the real and complex bi-adjoint models allow for trilinear interactions between the components through the δ couplings. We will see how the trilinear interaction can enhance dimension 5 effective couplings.

We now add a new dimension 5 effective operator through which the real bi-adjoint components may further interact with the Standard Model. At dimension 4, the (8,3,0) bi-adjoint has no allowable couplings to the Standard Model. In particular, quark couplings to $\overline{Q}_L^c Q_L$, which would conserve color and weak charge, are forbidden by hypercharge conservation. Our new operator will thus introduce the lowest dimension effective interaction by which the lightest bi-adjoint could decay.

This effective operator couples a single bi-adjoint scalar directly to the SU(2) and SU(3) field strength tensors. Our operator is

$$L = \frac{1}{\Lambda} \phi^{ij} W_{ij}^{\mu\nu} G_{\mu\nu}. \quad (7)$$

In equation 7 ϕ is the (8,3,0) bi-adjoint. The Roman letters indicate SU(2) indices while Greek letters indicate Lorentz indices. $W^{\mu\nu}$ is the SU(2) field strength tensor and $G_{\mu\nu}$ is the SU(3) field strength tensor. Λ is the effective cut-off of the operator. We see this operator has an effective dimension 5. After electroweak symmetry breaking, the SU(2) field strength tensor $W^{\mu\nu}$ will contain the W,Z and γ electro-weak gauge fields. We can see that this model thus presents an unusual operator in W-gluon sector of the di-boson portal, the portal through which new particles interact with the SM primarily through pairs of SM gauge bosons.

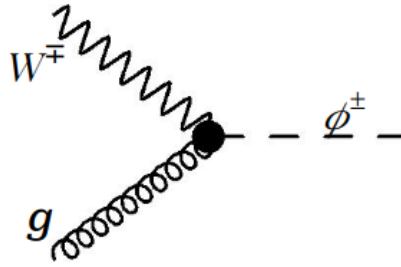
Expanding the above operator in components we extract the Lagrangian terms involving the charged bi-adjoints ϕ^\pm

$$\begin{aligned}
L \supset & (\partial^\mu A_3^\nu - \partial^\nu A_3^\mu)(\partial_\mu W_\nu^+ - \partial_\nu W_\mu^+)\phi^- + (\partial^\mu A_3^\nu - \partial^\nu A_3^\mu)(\partial_\mu W_\nu^- - \partial_\nu W_\mu^-)\phi^+ \\
& + eg_3 f^{abc} A_{3b}^\mu A_{3c}^\nu (\partial_\mu W_\nu^+ - \partial_\nu W_\mu^+)\phi^- + eg_3 f^{abc} A_{3b}^\mu A_{3c}^\nu (\partial_\mu W_\nu^- - \partial_\nu W_\mu^-)\phi^+ + \\
& \frac{iec_w}{s_w} (W_\mu^+ Z_\nu^0 - W_\nu^+ Z_\mu^0)(\partial^\mu A_3^\nu - \partial^\nu A_3^\mu)\phi^- + \frac{iec_w}{s_w} (W_\mu^- Z_\nu^0 - W_\nu^- Z_\mu^0)(\partial^\mu A_3^\nu - \partial^\nu A_3^\mu)\phi^+ + \\
& - ie(W_\mu^+ A_\nu - W_\nu^+ A_\mu)(\partial^\mu A_3^\nu - \partial^\nu A_3^\mu)\phi^- + ie(W_\mu^- A_\nu - W_\nu^- A_\mu)(\partial^\mu A_3^\nu - \partial^\nu A_3^\mu)\phi^+. \quad (8)
\end{aligned}$$

and the Lagrangian coupling involving the neutral bi-adjoints ϕ^0

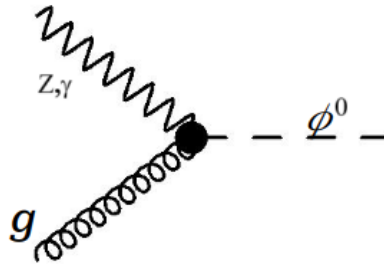
$$\begin{aligned}
s_W(\partial^\mu A_3^\nu - \partial^\nu A_3^\mu)(\partial_\mu A_\nu - \partial_\nu A_\mu)\phi^0 + c_W(\partial^\mu A_3^\nu - \partial^\nu A_3^\mu)(\partial_\mu Z_\nu - \partial_\nu Z_\mu)\phi^0 \\
s_w g_3 f^{abc} A_{3b}^\mu A_{3c}^\nu (\partial_\mu A_\nu - \partial_\nu A_\mu)\phi^0 - c_W g_3 f^{abc} A_{3b}^\mu A_{3c}^\nu (\partial_\mu A_\nu - \partial_\nu A_\mu)\phi^0 + \\
\frac{ie}{s_w} (W_\mu^+ W_\nu^- - W_\nu^+ W_\mu^-)(\partial^\mu A_3^\nu - \partial^\nu A_3^\mu)\phi^0. \quad (9)
\end{aligned}$$

In the Lagrangian above A_3 are the gluon fields and W^\pm are the W boson states and A is the photon. In the first line, we see we have direct three point interactions between the ϕ^\pm and a $W^\mp g$ pair.



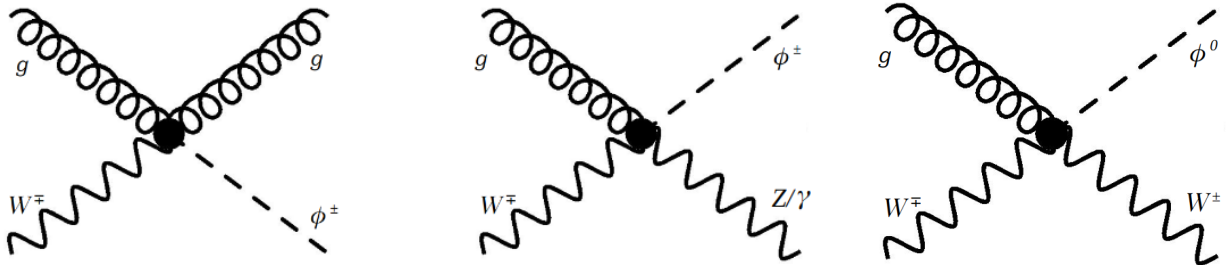
This interaction allows the direct decay of a charged ϕ^\pm into a W-gluon resonance. This interaction also allows a variety of new LHC production modes for charged bi-adjoints as we will later see.

There is a similar three point interaction for the neutral state ϕ^0 with one gluon and a neutral gauge boson (Z or γ).



This can allow the decay channel of a neutral state into a gluon-photon or gluon-Z resonance.

Starting on the second line of Equation 8 are the triple gauge boson interactions. On the second line of Equation 8 are interactions that couple a single charged ϕ^\pm to a W boson and two gluons. In the third and fourth lines, we find interactions that couple the charged components of ϕ to one gluon, one W boson and one neutral electroweak gauge boson (Z or photon). In Equation 9, we find an interactions that couple the neutral component ϕ^0 to various combinations of W bosons, neutral electroweak gauge bosons, and gluons. We represent these interactions as Feynman diagrams below.



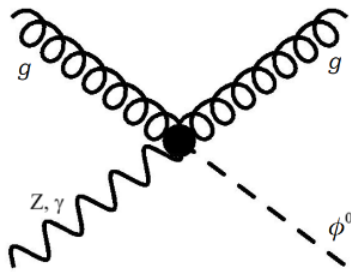


Figure 2. Feynman diagrams representing processes allowing access to an (8,3,0) LEX scalar involving 3 gauge bosons as described in (4).

The above interactions lead to a variety of interesting 2-2 and 2-3 collider production processes for the charged and neutral components of the bi-adjoint. In addition to these terms, the Lagrangian contains several 5-point interactions that couple the ϕ fields to 4 gauge bosons. These operators contribute to various 2-3 collider production processes that will not be the subject of this work.

This operator can be added alone to the dimension 5 theory as a stand alone operator generated by higher-energy physics. It will also receive a contribution in the tree level model, from a one loop triangle diagram involving the trilinear coupling of the adjoints $\delta\phi^3$. We re-iterate that this is lowest dimension effective operator through which the bi-adjoint can couple to the diboson portal, all other effective operators will require additional suppression by insertions of Higgs vevs to soak up SU(2) indices.

We note that we may add an equivalent operator

$$L = \frac{1}{\Lambda} \phi_I^{ij} \tilde{W}^{\mu\nu}_{ij} G_{\mu\nu} \quad (10)$$

which will allow similar interactions of the imaginary components of ϕ with the SU(2) and SU(3) field strength tensors. This will allow, for example, the decay of the pseudo-scalar states in the ϕ_I multiplet to decay to di-bosons pairs as well.

Parameter space benchmark

In this work we are interested in first analyzing some of the phenomenology of the simplest bi-adjoint model. We will thus choose to first analyze the real scalar model. Again in this there are three states, components of the real adjoint, which are CP even spin zero scalars. Further, the masses of these states are the same, $m_{\phi^+}^2 = m_{\phi^0}^2 = m_{\phi^-}^2$.

However, our conclusion will also apply to regions of the complex scalar model where the imaginary(pseudo scalar) bi-adjoints are much heavier than the real (scalar) bi-adjoints and are not easily accessible to LHC. LHC Production of the pseudo-scalar states can be achieved by moving their masses above into the 6 -7 TeV range, through their existence can still contribute to loop level decays of the scalar states. In this region of the complex model space we choose $\lambda_3 = \lambda_4 = 0$ which does not allow mass splitting between charged and neutral states and guarantees mass eigenstates are of definite CP. We can thus choose values of $m^2 > 0$ and $M^2 < 0$ with $|m^2| > |M^2|$ to avoid developing a ϕ vev. A fine tuning of order 10 percent between mass parameters will deliver 1-4 TeV masses for scalar components which pseudo-scalars remain above the 7 TeV scale.

The Higgs couplings in the real and complex models will induce one loop enhancements of Higgs couplings to gluons and Higgs couplings to di-photons [27]. In the (8,2,1) Manohar wise models, these effect appear to be compatible with Higgs production and decay measurements for exotic states above 1 TeV in mass for order one couplings [28][19]. We expect similar results in our model. However, we can consider all Higgs couplings to be zero in our very simplest bench mark point which mean the bi-adjoint make no one loop contributions to the Higgs di-boson couplings.

III. DECAYS OF THE BI-ADJOINTS

We now discuss the decay modes of the bi-adjoint components. The dimension 5 effective operator allows for a two-body resonant decay of the charged component to a W-boson and a gluon: $\phi^\pm \rightarrow W^\pm g$. This decay will make up 100% of the branching fraction of the charged bi-adjoint if the mass splitting between the charged and neutral components is zero.

The total decay width will be proportional to a factor of $\Gamma \sim m_{\phi^\pm}^3/\Lambda^2$. Below we plot the decay width of the lightest charged bi-adjoint in the Λ, m_{ϕ^\pm} parameter plane.

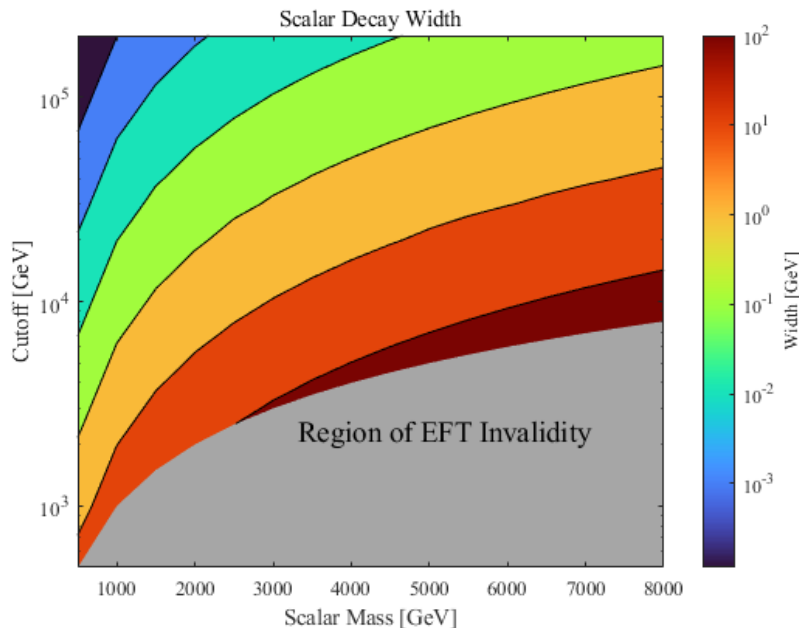


Figure 2 Decay width of the lightest ϕ^\pm in the Λ scalar mass plane.

Notice that in the region of very low effective cut-off, $\Lambda < m_{\phi^\pm}$, the effective operator validity breaks down. Therefore we see that the width increases at high mass and low effective cut-off but remains relatively narrow compared to the mass over the region of EFT validity.

The neutral component will always have available 2 body decay modes through the effective operator of $\phi_0 \rightarrow \gamma g$ and $\phi_0 \rightarrow Zg$. The relative decay widths of the gZ and $g\gamma$ decays are fixed by SU(2) gauge invariance. In principle the neutral component of the bi-adjoint can develop a decay width into di-gluons at loop level. This requires two Higgs insertion to soak up SU(2) indices so this happens through an effective operator of dimension 7. This means the any digluon decay will be suppressed compared to decays of the neutral states that result from dimension 5 operators. In the real adjoint model, the di-gluon coupling happens through a one loop process involving bi-adjoints in running in a triangle loop, however two conditions must be met for this coupling to be non-zero. First, the tri-linear coupling $\delta\phi^3$ must be non-zero, second the di-Higgs coupling must be non-zero. Similar gluon Z, gluon photon and digluon couplings and decays were studied for a slightly different dimension 5 operator model coupling to a pure color adjoint (8,1,0) in reference [11]. However this model also allowed the dimension 5 decay of a color adjoint to gluons, thus the digluon decay took up a much more substantial fraction of the branching ratio. In the (8,3,0) model without appreciable gluon decay branching fraction, the branching ratio of the neutral state of Z-gluon to γ gluon decays is $\sim c_w^2/s_w^2$ for heavy states, that is, the Z decays will dominate the branching fraction.

IV. LHC PRODUCTION MODES

We will now enumerate the most likely production modes for the (8,3,0) bi-adjoint field at the LHC.

Pair Production

Hadron colliders can always pair produce new states charged under the Standard Model gauge groups through gauge boson interaction terms that emerge from the exotic field's kinetic term. For color charged particles, the largest pair production cross section is from gluon fusion. In our case the production processes are $gg \rightarrow \phi^0\phi^0, \phi^+\phi^-$. Below we present the Feynman diagrams involved in the gluon fusion pair production of the bi-adjoint scalars.

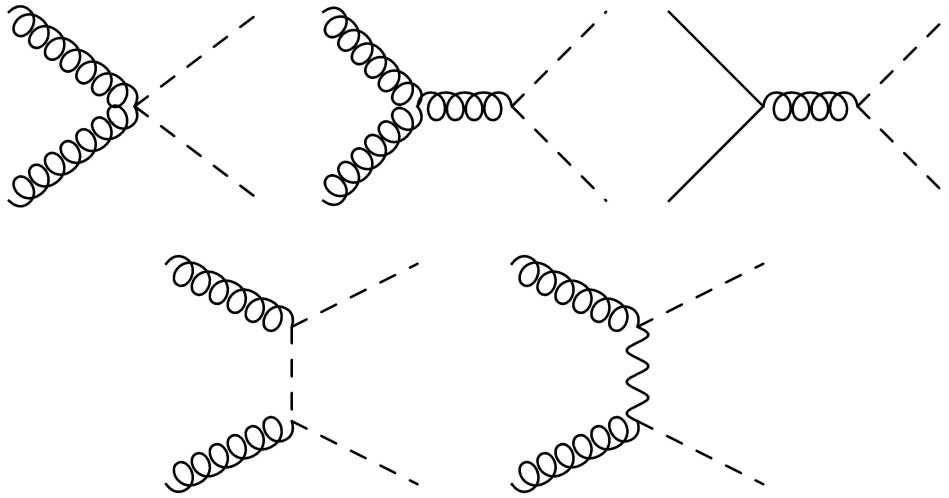


Figure 3 Pair Production modes of the (8,3,0) bi-adjoint from gluon fusion

We note that the new trilinear electroweak-gluon- ϕ^\pm vertex from the dimension 5 operator also makes a contribution the gluon fusion pair production through t-channel W exchange. This is the bottom right diagram in the figure above.

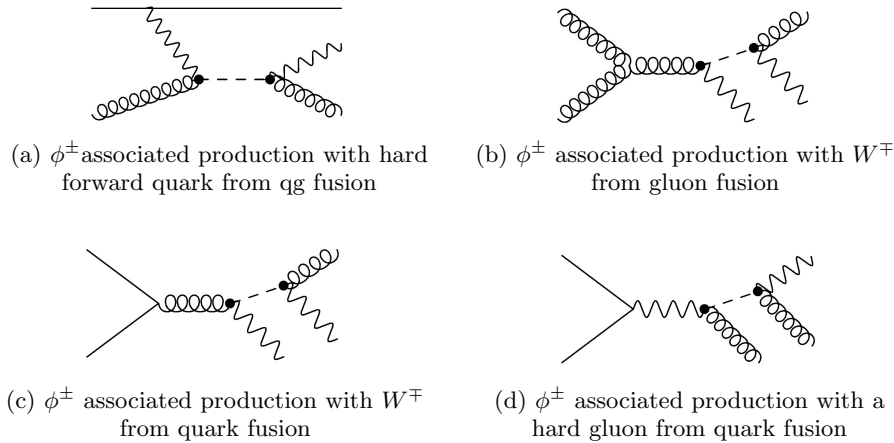


Figure 4 Single Production modes of the charged(8,3,0) bi-adjoint at LHC, with subsequent decay $\phi^\pm \rightarrow W^\pm g$.

Single Production of Charged Bi-Adjoint Scalars

We will now explore the single production modes of bi-adjoints at LHC. The effective dimension 5 operator allows a variety of single production modes for the charged and neutral bi-adjoint components. Here we will concentrate on the most probable 2-2 LHC processes in which a single bi-adjoint is produced in association with a one Standard Model particle. We will first focus on production of the charged ϕ^\pm states.

Figure 4 displays single-production modes of the lightest charged bi-adjoint, along with its subsequent decay back into W-gluon resonance.

Gluon Fusion

The first production mode we will discuss is the gluon fusion mode, where a single charged ϕ^\pm is produced with an associated W boson. Diagrams contributing to this process follow from the three point W-g ϕ vertex and 4 point ggW ϕ vertices of the dimension 5 operator. One of the gluon fusion diagrams may be seen in Figure 4b. The process is $gg \rightarrow W^\pm \phi^\mp$. Once the ϕ^\mp decays, events in this channel fall into 4 $W^\pm(W^\mp g)$ final states where there is one resonance (Wg).

Quark Fusion

There are two possible LHC quark fusion processes which produce a single charged ϕ^\pm . This first is quark fusion with W- ϕ associated production shown in Figure 4c. The full process is $q\bar{q} \rightarrow g^* \rightarrow W^\pm\phi^\pm$. In this process, same flavor quarks fuse into an off-shell gluon, and a $W^\pm\phi^\mp$ pair is created through the trilinear W-g- ϕ^\pm effective vertex. Once the ϕ^\pm decays, the final state topologies are again $W^\pm(W^\mp g)$ where the W's have either di-quark or lepton neutrino decay patterns.

The second quark fusion process produces a single ϕ^\pm in association with a hard gluon. This is illustrated in Figure 4d. The full process is $q\bar{q}' \rightarrow W^{\pm*} \rightarrow g\phi^\pm$. In this process a $q\bar{q}'$ pair fuse into an off-shell W boson which produces a final state gluon ϕ pair through the 3 point W-g- ϕ dimension 5 effective vertex. Once the ϕ^\pm decays the final state is $q\bar{q} \rightarrow g(W^\pm g)$, where the W and one hard gluon jet form a mass resonance. The subsequent decay of the W into jj or $l\nu$ pairs gives 4 final state topologies.

Quark-Gluon Fusion

The final single production mode is an interesting asymmetric process which produces a ϕ^\pm in association with a hard forward quark jet. The process can be seen in Figure 4a. In this t-channel quark-gluon fusion process the initial state gluon fuses with an off-shell W radiated by the incoming quark. The three point W-g- ϕ vertex produces a single ϕ in addition to the hard forward quark. The process is $qg \rightarrow q'\phi^\pm$. Once the ϕ^\pm decays to a W gluon resonance, the process is $qg \rightarrow q'(W^\pm g)$, where the W and hard gluon form a resonance. With W decays to di-jets or lepton-neutrino pairs, there are two final state event topologies.

Cross Section Comparison

We have plotted comparisons of various charged ϕ^\pm production cross section for 14 TeV LHC. To produce these cross sections we have used FeynRules [29][30] to implement Lagrangian interactions from section 2 and generate UFO output [31]. We then used Madgraph5@NLO[32] to generate cross sections for 5 production processes. These include pair production from gluon fusion and four single production channels, $qg \rightarrow \phi q$, $gg \rightarrow \phi W$, $q\bar{q} \rightarrow \phi W$, and $q\bar{q} \rightarrow \phi g$. We plot cross sections for a benchmark choice of effective cut off $\Lambda = 5$ TeV.

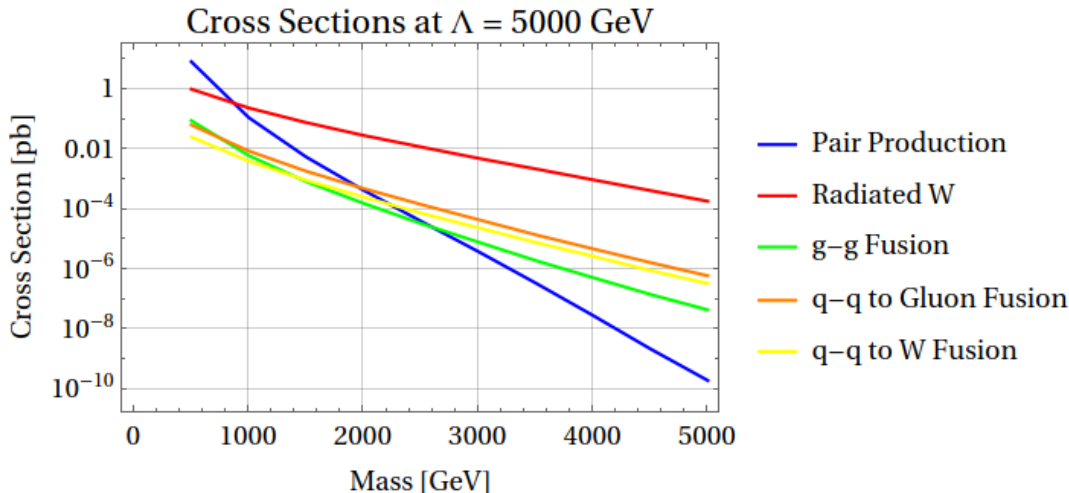


Figure 5 Comparison of the cross section vs ϕ^\pm mass for 5 production processes. $\Lambda = 5$ TeV and $m_{\phi^+} = m_{\phi^-}$.

We find that the pair production cross section only dominates over single production for low masses of ϕ around 800 GeV. The pair production cross section drops off somewhat dramatically as the scalar mass increases due to the kinematic suppression of two high mass final state particles. For 10 TeV effective cut-off we find a similar feature with single production taking over just after the 1 TeV threshold. The single production mode maintains more kinematic phase space at high bi-adjoint mass so that for most of the multi-TeV parameter space, single production is the leading process.

The single production mode that clearly dominates is the the quark-gluon process $qg \rightarrow q' + \phi$, which fuses an off-shell W with the incoming gluon. This cross section beats that of the other single production modes at all masses

and cutoffs tested. We note that in the quark gluon fusion channel single production cross sections of the bi-adjoint remain above the fb range for 3-4 TeV particle masses.

In addition to the difference in cross sections, we expect the single production mode involving a radiated boson to create a distinctive signal asymmetric signal at LHC as we expect a massive ϕ^\pm and a hard forward jet. These events will also have a distinctive W-gluon resonant feature. Due to these reasons, we propose a single production HL-LHC search in this channel later in the paper.

Neutral States

Single production modes for the neutral gauge boson are similar to those involving the charged gauge boson but with neutral Z and γ electroweak boson appearing in final states rather than W bosons. We give a schematic of the LHC single production modes in the diagram below.

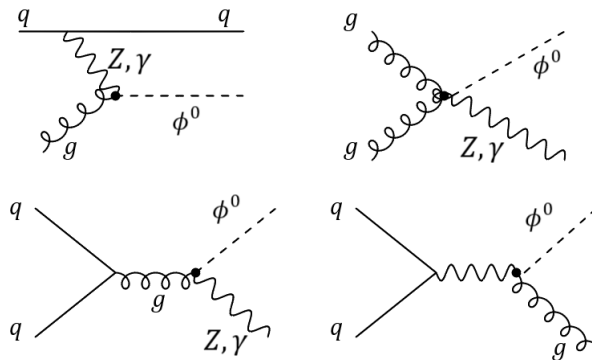


Figure 6 LHC single production modes of neutral bi-adjoints

The quark gluon fusion mode leads to the production of a ϕ^0 in association with a final state Z or γ through the process $gg \rightarrow \phi^0 + Z/\gamma$. An example diagram is shown in Figure 6b. Quark fusion also yields $\phi^0 Z$ and $\phi^0 \gamma$ final states through quark fusion into an off-shell gluon. This is demonstrated in Figure 6c with the process $q\bar{q} \rightarrow g^* \rightarrow \phi^0 + Z/\gamma$. Separate quark fusion processes yield a $\phi^0 g$ final state through quark fusion through an off-shell Z or γ in Figure 6d. Finally, the t-channel quark gluon process gives a $\phi^0 + q$ final state as an incoming gluon fuses with a neutral gauge boson radiated off of the initial state quark. This process is shown in Figure 6a and is $qg \rightarrow q + \phi^0$. The production processes are generally smaller for neutral bi-adjoints than for the charged states, especially the quark and gluon associated production processes which contain off-shell photons and Zs. There are several promising LHC signatures with final state photons such as the gluon fusion process $gg \rightarrow \gamma \phi^0 \rightarrow \gamma(g\gamma)$.

V. LHC SEARCH FOR CHARGED BI-ADJOINTS

In this section we propose a new HL-LHC search for the single production of the charged bi-adjoint field. This search makes use of the most probable single production mode for ϕ^\pm and its distinctive W-gluon resonant decay. We propose a search in the quark gluon fusion channel where ϕ^\pm is produced in association with a hard forward jet. The ϕ^\pm then decays to a W-gluon resonance with the total process $qg \rightarrow q' \phi^\pm \rightarrow W^\pm g + j$. In the figure below we show the Feynman diagram giving the total production and decay for this process.

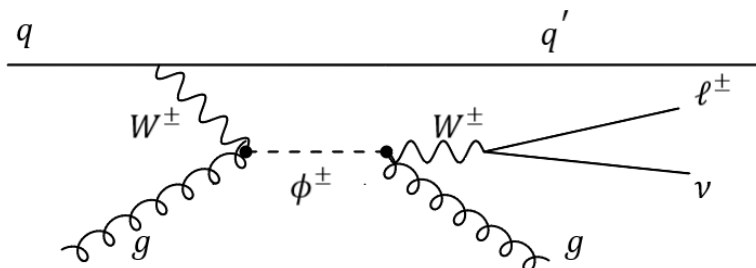


Figure 7 Associated production of ϕ^\pm and forward jet with subsequent decay $\phi^\pm \rightarrow W^\pm g \rightarrow \ell^\pm \nu g$

For our search we will consider leptonic decays of the bi-adjoint $\phi^\pm \rightarrow W g \rightarrow \ell^\pm \nu g$ with the process. The full process is

$$qg \rightarrow q' \phi^\pm \rightarrow W^\pm g + j \rightarrow \ell^\pm \nu g + q$$

This is a quite probable final state for the search, as the leptonic branching fraction of the W is ~ 20 percent.

There are many distinctive features of this process. First, it contains both missing energy and a single hard lepton. It has a hard forward jet. It also has a very hard gluon jet emanating from the decay of the multi-TeV ϕ particle with characteristic p_T peaking at about half of the ϕ mass. Finally, the leading jet and lepton have a transverse mass that has a kinematic edge at the mass of the ϕ^\pm particle.

Below we contour-plot 14 TeV LHC production cross sections for the $qg \rightarrow \phi^\pm q'$ process in the m_{ϕ^\pm}, Λ mass plane. Cross sections are computed with Madgraph5@NLO and scaled by a modest k-factor of 1.3. In these simulations we use a simple benchmark model scenario where the charged bi-adjoint is a CP even scalar, $m_{\phi^+} = m_{\phi^-}$ and charged bi-adjoints have W-gluon as their only decay mode.

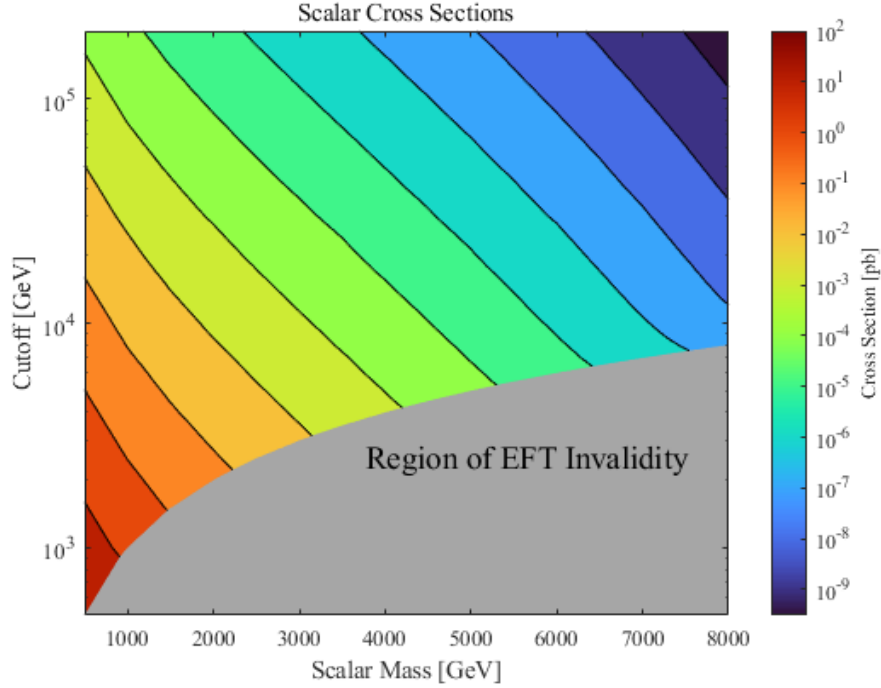


Figure 8 Combined cross sections for the single production channel $qg \rightarrow q + \phi^\pm$ in the m_{ϕ^\pm}, Λ plane. We note the region $\Lambda < m_{\phi^\pm}$ where the EFT becomes invalid.

We see, of course, that the production cross section falls off with increasing scalar mass. The overall production cross section falls as $1/\Lambda^2$. However we maintain appreciable LHC production cross section for quite massive ϕ^\pm , into the 4 TeV range. Production cross sections also remain appreciable for effective cut-offs in of order 10s of TeV. In the plot we have noted the region of low effective cut-off $\Lambda < m_{\phi^\pm}$ where the EFT becomes invalid.

Search Criteria

We now institute a sensitivity study for the single bi-adjoint production channel $qg \rightarrow \phi^\pm + q' \rightarrow \ell^\pm \nu g + q'$ for the complete $3ab^{-1}$ run of HL-LHC. We require at least two hard jets, exactly one hard lepton and missing energy in our events. We institute the following pre-selection search criteria for event generation

Pre-selection Criteria

- events must has 2 hard jets $p_T > 30 GeV$
- events must contain significant missing energy $E_T^{miss} > 70 GeV$

- events must contain exactly one hard isolated lepton $p_T > 10\text{GeV}$

We then impose further cuts creating low, medium, and high mass search regions. These search regions include thresholds for reconstructed transverse mass of the leading jet-lepton pair $m_{T_{j1\ell}}$. They also include and an increasing p_T threshold for the leading and subleading jets.

In the low mass region we require

- $E_T^{miss} > 140\text{ GeV}$
- p_T leading jet $> 180\text{ GeV}$
- p_T sub-leading jet $> 85\text{ GeV}$
- $m_{T_{j1\ell}} > 700\text{ GeV}$

In the intermediate mass region we require a slightly higher threshold for the leading and sub-leading jets. In this intermediate region we use a sliding window of transverse mass thresholds for leading jet-lepton pair that cuts the region into 6 bins.

- $E_T^{miss} > 140\text{ GeV}$
- p_T leading jet $> 200\text{ GeV}$
- p_T sub-leading jet $> 110\text{ GeV}$
- $m_{T_{j1\ell}}$ in 6 bins between 1100 and $> 2350\text{ GeV}$

In the high mass region we use a single stringent high mass threshold on the transverse mass

- $E_T^{miss} > 1400\text{ GeV}$
- p_T leading jet $> 200\text{ GeV}$
- p_T sub-leading jet $> 110\text{ GeV}$
- $m_{T_{j1\ell}} > 2400\text{ GeV}$

The leading backgrounds for this process are $t\bar{t}$ and W +jets with leptonic decay of the W . Other important backgrounds include the di-boson processes $WW/ZZ/WZ$. Smaller but still significant backgrounds include and the asymmetric processes of qt and Wt production.

Below we list background production cross sections for the 5 background processes for 14 TeV c.o.m energy at LHC. Background events were created with Madgraph5@NLO, showered with Pythia [33] and run through DELPHES detector simulation [34]. These cross sections were computed at leading order with Madgraph5@NLO and scaled by listed k-factors using a 70 GeV missing energy pre-selection threshold. We used background samples 1850k, W +j events, 1150k $t\bar{t}$ events, 500k diboson events, 400k qt events, and 200k Wt events.

Background Process	Cross Section (pb)	K-Factor Used
$t\bar{t}$	888.78	1.489
W + jets	1361	1.401,1.234
Diboson	441.7	1.417,1.316,1.599
qt	51.84	1.29
tW	91.742	1.4

Leading Order cross sections in 5 background channels generated by MadGraph5@NLO and scaled by appropriate K factor. A preselection cut of $\text{MET} > 70$ was applied in event generation.

We have created kinematic distributions for several discriminants in our LHC process. Implementing the Lagrangian in section 2 with Feynrules we output UFO files to Madgraph5@NLO for event generation. We showered events with Pythia and used DELPHES detector simulation. Distributions bins were created using MadAnalysis. Background simulations were done at leading order with Madgraph5@NLO, showered with Pythia run through DELPHES detector simulation and binned with Madanalysis[35].

In Figure 9 below we plot p_T distributions for the leading jets in the signal and background events. Signal events are plotted for four ϕ^\pm mass benchmarks of 500 GeV, 1 TeV, 3 TeV, and 5 TeV.

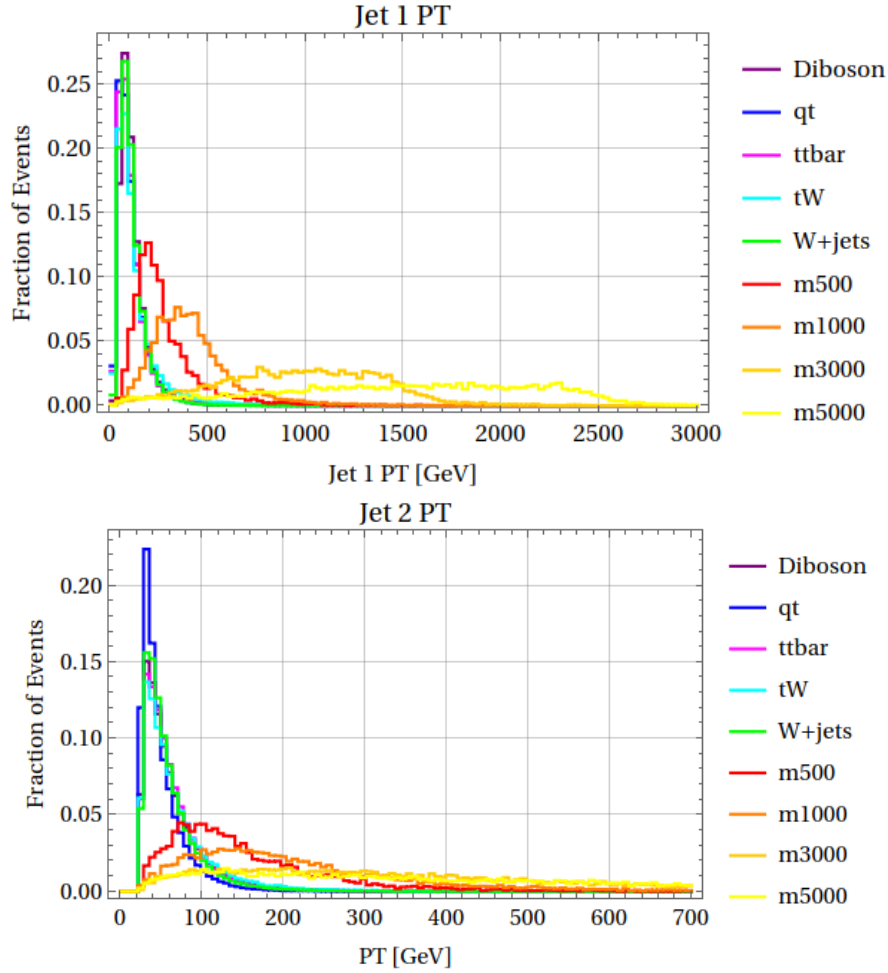


Figure 9 Above)quark and Below) gluon transverse momentum distributions. in 14 TeV LHC $qg \rightarrow \phi^\pm + q$ events. Distributions are made with three benchmark ϕ^\pm masses 500 GeV(blue), 2 TeV (orange), and 5 TeV (green).

In the signal events the leading jet,most likely the gluon emanating from the two body decay of the ϕ^\pm , has a characteristic peak at half of the ϕ^\pm mass. This characteristic p_T becomes extremely substantial at high ϕ^\pm mass. The transverse momentum of the sub-leading jet in the signal events, the associated quark jet, remains characteristically lower over a large range of ϕ^\pm masses. This jet is forward and has small component in the transverse direction. However the characteristic peak for this jet occurs in the hundred GeV range for low masses, but becomes substantially distributed over a few hundred GeV range for high mass bi-adjoint events. By contrast, the leading and sub-leading jets in the background peak at extremely low momentum and do not extend substantially into the few hundred GeV range.

We have plotted the missing energy distribution of signal and background events in figure 10. The plots show the missing energy vs. the fraction of events on an Above) log and Below) Linear scale. Signal events were plotted at four mass benchmarks 500 GeV, 1 TeV, 3 TeV, and 5 TeV.

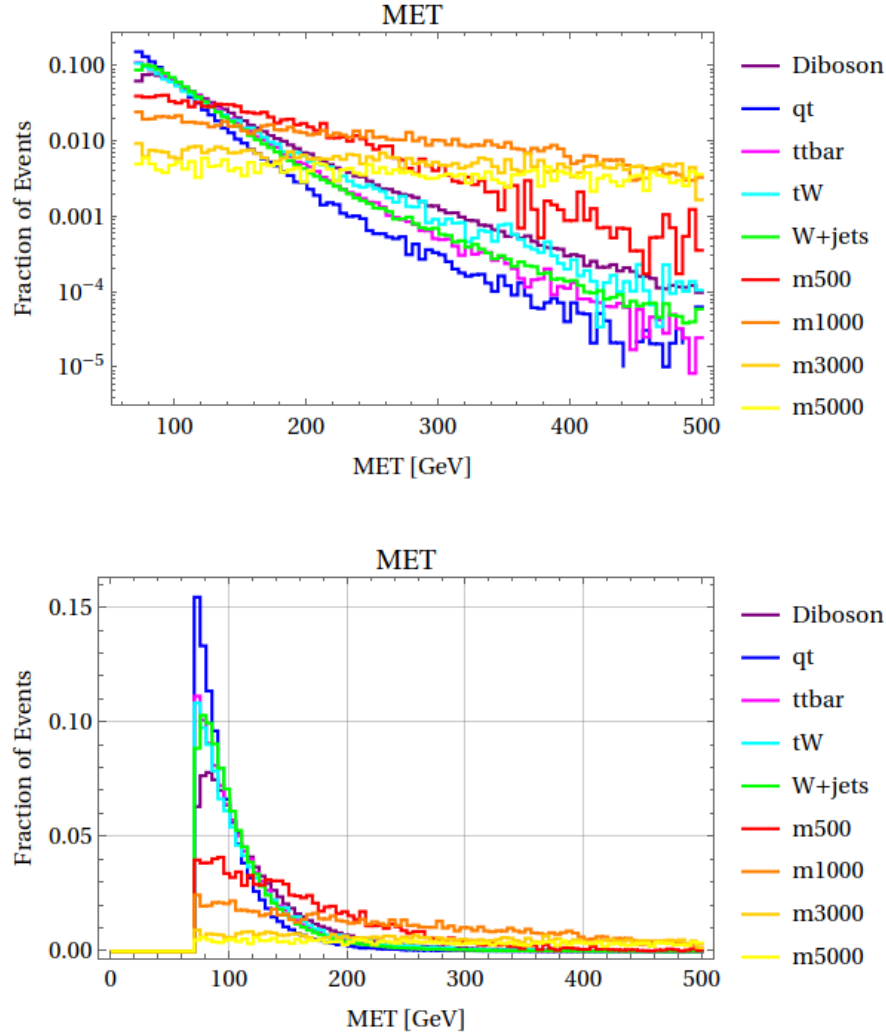


Figure 10 Above)Log and Below) Linear plots of missing energy distributions for signal and background events at 14 TeV LHC. Distributions are made with four benchmark ϕ^\pm masses 500 GeV, 1 TeV, 3 TeV, and 5 TeV.

The signal events have greater event fraction at higher missing energy thresholds. The high missing energy fraction of events increases with increasing bi-adjoint mass. The qt, ttbar, and tW background are monotonically decreasing, while diboson and W+jets backgrounds peak at low MET thresholds and dramatically fall, with all background very suppressed for missing energies above 140 GeV.

We also plot the transverse mass distribution of the leading jet-lepton pair. We plot the distribution for signal and background events for four ϕ^\pm masses, 500 GeV, 1 TeV, 3 TeV and 5 TeV.

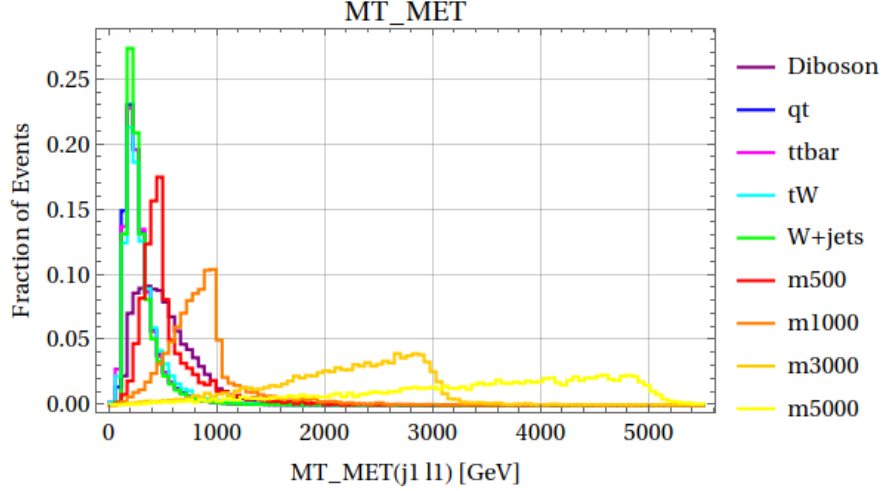


Figure 11 Plot of the leading jet-lepton transverse mass distribution for signal and background events at 14 TeV LHC. Distributions are made with four benchmark ϕ^\pm masses 500 GeV, 1 TeV, 3 TeV, and 5 TeV.

We see that the signal events display a kinematic peak and edge at the transverse mass threshold corresponding to the bi-adjoint mass. The high mass signal events are noticeably flatter than low mass events with smearing of the edge, but the feature is still easily discernible. The backgrounds, with the notable exception of the di-boson background peak around the 100 GeV threshold, with the diboson background peaking at slightly a higher threshold, significantly overlapping with the 500 GeV signal events.

We plot lepton p_T distributions for the signal and backgrounds in figure 11 below. We plot the distribution for bi-adjoint masses of 500 GeV, 1 TeV, 3 TeV and 5 TeV.

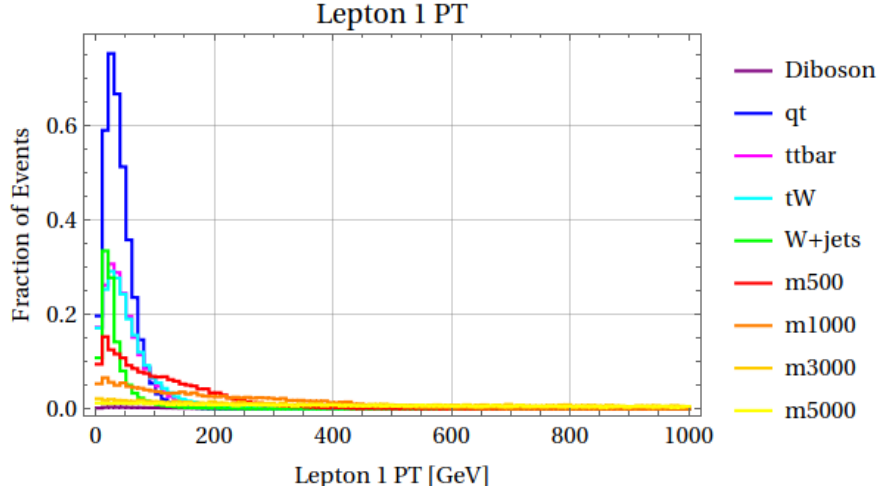


Figure 12 Plot of the lepton p_T distribution for signal and background events at 14 TeV LHC. Distributions are made with four benchmark ϕ^\pm masses 500 GeV, 1 TeV, 3 TeV, and 5 TeV.

We see that while both signal and background lepton p_T peaks at low momentum, there is an appreciable spread of higher p_T lepton events in the signal samples. The lepton p_T distribution of the signal events shows a considerable flattening higher bi-adjoint masses.

We will now show efficiencies of our search criteria for signal and background events. In the table I below we give the cut flows for signal events in the the bi-adjoint search. The table shows the cut-flows for the low, medium, and high mass search ranges. We give efficiencies of each selection cut for various ϕ^\pm mass values. The efficiencies in the low and high mass search regions follow the general pattern of increasing with increasing bi-adjoint mass. In the low search region, the lightest mass events do worse at passing the 140 GeV missing energy cut and transverse mass threshold. Efficiencies in the tighter $m_{T_{j1\ell}}$ binned medium-mass search region hold steady with an efficiency in the low 30 percent range. Signal events in the high mass search region do better at passing the 2.4 TeV transverse mass threshold as the bi-adjoint mass is increased.

Low Mass Region, $\sqrt{s} = 14$ TeV, labeled by m_Φ [GeV]

Selection criterion	500	750	1000	1250
$E_T^{\text{miss}} > 140$	0.292	0.447	0.529	0.604
$p_T(j_1) > 180$ GeV	0.251	0.396	0.496	0.580
$p_T(j_2) > 85$ GeV	0.171	0.337	0.435	0.522
$m_{T_{j_1 l_1 \text{MET}}} > 700$ GeV	0.0614	0.161	0.336	0.462

Mid-mass Region , $\sqrt{s} = 14$ TeV, labeled by m_Φ [GeV]

Selection criterion	1500	1750	2000	2250	2500	2750
$E_T^{\text{miss}} > 140$	0.6477	0.68416	0.7214	0.7401	0.7651	0.7843
$p_T(j_1) > 200$ GeV	0.6188	0.6586	0.6979	0.7187	0.7438	0.76258
$p_T(j_2) > 110$ GeV	0.5307	0.5689	0.6127	0.6350	0.65688	0.68241
$m_{T_{j_1 l_1 \text{MET}}} [\text{GeV}]$	1100	1300	1500	1650	1850	2350
Final $m_{T_{j_1 l_1 \text{MET}}}$ cut	0.328818	0.3305	0.3443	0.363416	0.35746	0.23568

High Mass Region, $\sqrt{s} = 14$ TeV, labeled by m_Φ [GeV]

Selection criterion	3000	3500	4000	4500	5000
$E_T^{\text{miss}} > 140$	0.7899	0.8199	0.8327	0.8496	0.8640
$p_T(j_1) > 200$ GeV	0.7701	0.8002	0.8074	0.8275	0.8375
$p_T(j_2) > 110$ GeV	0.6830	0.7110	0.7206	0.7385	0.7456
$m_{T_{j_1 l_1 \text{MET}}} > 2400$	0.2952	0.4373	0.5252	0.5826	0.6240

TABLE I: Cut-flows for signal samples in proposed search for scalar bi-adjoint. Results apply to center-of-mass energy $\sqrt{s} = 14$ TeV. Efficiencies are cumulative after each selection cut.

Efficiencies for $t\bar{t}$, W +jets, diboson, qt and tW backgrounds are found in table 3. The upper table presents cut flows for 5 backgrounds in the low-mass search region. The lower table presents the intermediate mass and high mass search regions. In the low mass search region final background efficiencies for the leading backgrounds are in the .1 percent range. In the intermediate and high mass search regions the transverse mass cut is extremely powerful for suppressing background with W plus jets suppression of order 10^{-5} .

Implementing these search criteria for the full $3ab^{-1}$ data set for the HL-LHC. We compute the significance as

$$S = \frac{N_{\text{signal}}}{\sqrt{N_{\text{bkg}}}} \quad (11)$$

Light Cuts, $\sqrt{s} = 14$ TeV, Background Efficiencies

Selection criterion	$t\bar{t}$	W+jets	Diboson	qt	tW
$E_T^{\text{miss}} > 140$	0.0369	0.144	0.231	0.0267	0.0434
$p_T(j_1) > 180$ GeV	0.00954	0.0585	0.0852	0.0125	0.0167
$p_T(j_2) > 85$ GeV	0.0049	0.0271	0.0411	0.00166	0.0082
$m_{T_{j_1 l_2 \text{MET}}} > 700$ GeV	0.00103	0.00732	0.00267	0.000556	0.00252

Mid- and High-Mass Cuts, $\sqrt{s} = 14$ TeV, Background Efficiencies

Selection criterion	$t\bar{t}$	W+jets	Diboson	qt	tW
$E_T^{\text{miss}} > 140$	0.0369	0.144	0.231	0.0267	0.0434
$p_T(j_1) > 200$ GeV	0.00766	0.0467	0.0677	0.0104	0.0144
$p_T(j_2) > 110$ GeV	0.00303	0.0172	0.0259	8.98e-04	0.00537
$m_{T_{j_1 l_1 \text{MET}}} > 1100$ GeV	1.69e-04	0.00133	3.96e-04	9.50e-05	6.42e-04
$m_{T_{j_1 l_1 \text{MET}}} > 1300$ GeV	8.01e-05	6.52e-04	2.06e-04	4.40e-05	4.09e-04
$m_{T_{j_1 l_1 \text{MET}}} > 1500$ GeV	4.14e-05	3.49e-04	1.21e-04	2.39e-05	2.16e-04
$m_{T_{j_1 l_1 \text{MET}}} > 1650$ GeV	2.02e-05	2.06e-04	7.77e-05	1.80e-05	1.67e-04
$m_{T_{j_1 l_1 \text{MET}}} > 1850$ GeV	9.22e-06	1.15e-04	4.61e-05	1.20e-05	1.40e-04
$m_{T_{j_1 l_1 \text{MET}}} > 2350$ GeV	2.77e-06	2.00e-05	1.43e-05	6.25e-06	2.07e-05
$m_{T_{j_1 l_1 \text{MET}}} > 2400$ GeV	1.84e-06	2.00e-05	1.07e-05	3.02e-06	2.07e-05

TABLE II: Efficiencies of the backgrounds after cuts for each region.

with the statistical uncertainty of the background as the uncertainty. In Figure 13 we plot the $3^{ab^{-1}}$ HL-LHC 5σ (blue) discovery potential and 2σ (red) sensitivity in the m_{ϕ^\pm}, λ plane. Note that exclusions apply to the regions of EFT validity in the parameter space *where* $\Lambda > m_{\phi^\pm}$, or where the effective cut-off is greater than m_{ϕ^\pm} , roughly the the minimum allowable center of mass energy of the events.

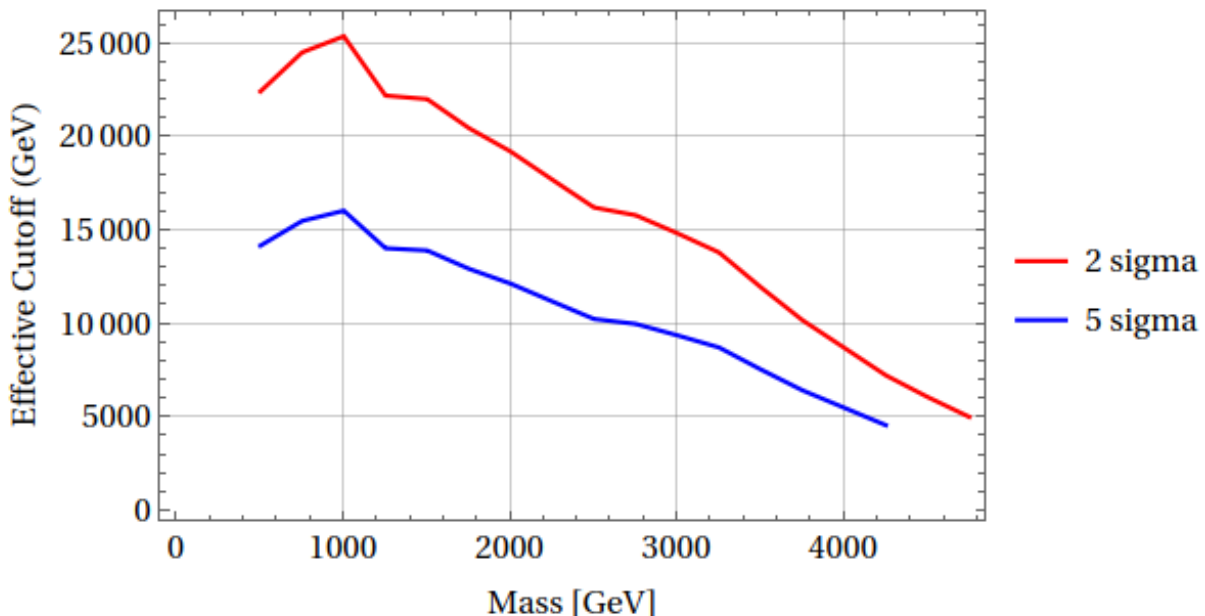


Figure 13 5 sigma discovery potential and 2 sigma exclusions for charged bi-adjoints ϕ^\pm in $3ab^{-1}$ at HL-LHC

The 5σ reach of the LH-LHC extends to 3-TeV bi-adjoints with effective cut-offs near the $\Lambda = 10$ TeV range. Discovery potential extends up to 4 TeV for $\Lambda = 5$ TeV though this heavier region is near the limit of the effective operator paradigm. The 2σ sensitivity potential extends up to 19 TeV effective cut-offs for 2 TeV bi-adjoint masses and around 15 TeV effective cut-offs for 3 TeV bi-adjoint masses. The 2 sigma sensitivity extends to effective cut-offs of 5 TeV for 4.75 TeV bi-adjoints.

VI. CONCLUSIONS

We have explored several new LHC production modes for a CP-even exotic scalar which is a bi-adjoint under the Standard Model SU(3) and SU(2), where the field couples to the SU(2) and SU(3) field strength tensors through a new dimension 5 effective interaction. We have shown how the single production of this exotic state is the dominant collider production mode for masses above a TeV for and cut-off in the 10 TeV range. We have explored the LHC production cross sections of this state in single production channels from quark and gluon fusion. We have also introduced a new search in an asymmetric W-gluon fusion production channel where a single ϕ is produced in association with a hard forward jet. We showed how this production channel is the dominant production mode of the charged ϕ states introduced a new HL-LHC search for a scalar produced in this mode with a decay to a gluon-W resonance. We find 5-sigma discovery potential for scalar masses up 3 TeV for cut-offs of 10 TeV, and two-sigma sensitivity for masses up to 3 TeV effective cut-offs up to the 15 TeV and 4 TeV masses up to 3.8 TeV.

There are several new directions that could be pursued to follow up on this work. Most interesting would be deeper phenomenological analysis of the complex bi-adjoint model. 1-4 TeV pseudoscalar states will generally have high LHC production cross sections [36] In particular, it would be interesting to explore cascade decays in different mass splitting regions of the parameter space. This would be especially interesting in regions where a pseudo-scalars sector is kinematically accessible. It would be interesting to explore a full effective operator catalog for the bi-adjoint to see if other couplings to the Standard Model are possible with alternate phenomenology. Further precision analysis of this parameter space may yield interesting results for Higgs production and decay as well as for electroweak precision. In fact the authors were successful in fitting recently fashionable electroweak parameters with exotic color charged particles[37]. Other avenues involve building UV completions of the dimension 5 operator that couple the bi-adjoint to the Standard Model.

It would also be interesting to use the W-gluon fusion process we have explored as a search channel for other exotic states that could be accessed through the W-gluon portal such as the (8,2,1) Manohar-Wise field and the (8,4,-1) SU(2) quadruplet field. These states also have a varied phenomenology with various mass hierarchy regimes between field components, and interesting possibilities for cascade decays.

Appendix: Quartic Interactions of the Bi-adjoint

We briefly discuss quartic terms that can appear in the bi-adjoint Lagrangian. Due to the nature of the bi-adjoint SM gauge charged, there is a large multiplicity of possible bi-adjoint quartic terms. Recalling SU(3) tensor product rules we have [38][39]

$$8 \otimes 8 = 1 \oplus 8 \oplus 8_s 10_s \oplus \overline{10}_s \oplus 27 \quad (12)$$

The 10 is an 3 index symmetric object. The 27 has two upper and two lower symmetrized indices.

Similarly, we have the tensor product rule for two adjoints of SU(2)

$$3 \otimes 3 = 1 \oplus 3 \oplus 5 \quad (13)$$

where the 5 of SU(2) is the four index symmetric object.

We see we have 12 possible contractions of the SU(3) and SU(2) indices of 4 bi-adjoint fields. To categorize the different SU(2) and SU(3) contractions we use lower case roman letters to indicate the fundamental SU(2) indices of the fields. We also indicate fundamental SU(3) indices of bi-adjoint bilinears with Greek letters.

For the real model we can categorize these quartics

$$\begin{aligned} L \supset & y_1(\phi_{ij}\phi^{ij})(\phi_{lk}\phi^{kl}) + y_2(\phi_i^j\phi_j^k)(\phi_k^l\phi_l^i) + y_3(\phi_{ij}\phi_{kl})(\phi^{ij}\phi^{kl}) + \\ & y_4(\phi_{ij}\phi^{ij})_\alpha^\beta(\phi_{kl}\phi^{kl})_\beta^\alpha + y_5(\phi_i^j\phi_j^k)_\alpha^\beta(\phi_k^l\phi_l^i)_\beta^\alpha + y_6(\phi_{ij}\phi_{kl})_\alpha^\beta(\phi^{ij}\phi^{kl})_\beta^\alpha \\ & y_7(\phi_{ij}\phi^{ij})_{\gamma\delta}^{\alpha\beta}\epsilon_{\alpha\beta\rho}(\phi_{kl}\phi^{kl})_{\alpha\beta}^{\gamma\delta}\epsilon^{\alpha\beta\rho} + y_8(\phi_i^j\phi_j^k)_{\gamma\delta}^{\alpha\beta}\epsilon_{\alpha\beta\rho}(\phi_k^l\phi_l^i)_{\alpha\beta}^{\gamma\delta}\epsilon^{\alpha\beta\rho} + y_9(\phi_{ij}\phi_{kl})_{\gamma\delta}^{\alpha\beta}\epsilon_{\alpha\beta\rho}(\phi^{ij}\phi^{kl})_{\alpha\beta}^{\gamma\delta}\epsilon^{\alpha\beta\rho} \\ & y_{10}(\phi_{ij}\phi^{ij})_{\alpha\beta}^{\gamma\delta}(\phi_{kl}\phi^{kl})_{\gamma\delta}^{\alpha\beta} + y_{11}(\phi_i^j\phi_j^k)_{\alpha\beta}^{\gamma\delta}(\phi_k^l\phi_l^i)_{\gamma\delta}^{\alpha\beta} + y_{12}(\phi_{ij}\phi_{kl})_{\alpha\beta}^{\gamma\delta}(\phi^{ij}\phi^{kl})_{\gamma\delta}^{\alpha\beta} \quad (14) \end{aligned}$$

The complex representation has more possible quartics and both ϕ and ϕ^\dagger can appear in quartic terms. There are three types of terms plus their hermitian conjugates

$$\phi^4, \phi^2\phi^{\dagger 2}, \phi\phi^{\dagger 3} + h.c. \quad (15)$$

for a total of 36 terms whose group theory structure follows the equation above.

Acknowledgments

This work was partially supported by the OSU department of Physics

Statement of Human Authenticity

The authors affirm that all text, images, and conceptual creation put forward in this work are entirely human generated, with no input from generative artificial intelligence (AI). The authors do not consent to the use of this work in the training of generative AI models.

-
- [1] L. M. Carpenter, T. Murphy, and M. J. Smylie, *LEX-EFT: the Light Exotics Effective Field Theory*, *JHEP* **08** (2023) 050, [[arXiv:2302.01344](#)].
 - [2] L. M. Carpenter, K. Schwind, and T. Murphy, *Leptonic signatures of color-sextet scalars. II. Exploiting unique large-ETmiss signals at the LHC*, *Phys. Rev. D* **109** (2024), no. 7 075010, [[arXiv:2312.09273](#)].
 - [3] L. M. Carpenter, T. Murphy, and K. Schwind, *Leptonic signatures of color-sextet scalars*, *Phys. Rev. D* **106** (2022), no. 11 115006, [[arXiv:2209.04456](#)].
 - [4] L. M. Carpenter, T. Murphy, and T. M. P. Tait, *Phenomenological cornucopia of SU(3) exotica*, *Phys. Rev. D* **105** (2022), no. 3 035014, [[arXiv:2110.11359](#)].
 - [5] L. M. Carpenter and K. Schwind, *Unusual portals to new exotics, the W-gluon portal*, [arXiv:2410.08195](#).
 - [6] L. M. Carpenter, M. J. Smylie, J. M. C. Ramirez, C. McDowell, and D. Whiteson, *New physics in triboson event topologies*, *Phys. Rev. D* **105** (2022), no. 7 075027, [[arXiv:2112.00137](#)].

- [7] E. C. F. S. Fortes, K. S. Babu, and R. N. Mohapatra, *Flavor Physics Constraints on TeV Scale Color Sextet Scalars*, in *6th International Workshop on Charm Physics*, 11, 2013. [arXiv:1311.4101](#).
- [8] T. Han, I. Lewis, and Z. Liu, *Colored Resonant Signals at the LHC: Largest Rate and Simplest Topology*, *JHEP* **12** (2010) 085, [[arXiv:1010.4309](#)].
- [9] T. Han, I. M. Lewis, H. Liu, Z. Liu, and X. Wang, *A guide to diagnosing colored resonances at hadron colliders*, *JHEP* **08** (2023) 173, [[arXiv:2306.00079](#)].
- [10] A. V. Manohar and M. B. Wise, *Flavor changing neutral currents, an extended scalar sector, and the Higgs production rate at the CERN LHC*, *Phys. Rev. D* **74** (2006) 035009, [[hep-ph/0606172](#)].
- [11] L. M. Carpenter and R. Colburn, *Searching for Standard Model Adjoint Scalars with Diboson Resonance Signatures*, *J. High Energy Phys.* **12** (2015) 151, [[arXiv:1509.07869](#)].
- [12] C.-Y. Chen, A. Freitas, T. Han, and K. S. M. Lee, *Heavy Color-Octet Particles at the LHC*, *J. High Energy Phys.* **05** (2015) 135, [[arXiv:1410.8113](#)].
- [13] M. Gerbush, T. J. Khoo, D. J. Phalen, A. Pierce, and D. Tucker-Smith, *Color-octet scalars at the CERN LHC*, *Phys. Rev. D* **77** (2008) 095003, [[arXiv:0710.3133](#)].
- [14] T. Plehn and T. M. P. Tait, *Seeking Sgluons*, *J. Phys. G* **36** (2009) 075001, [[arXiv:0810.3919](#)].
- [15] G. Cacciapaglia, A. Deandrea, T. Flacke, and A. M. Iyer, *Gluon-Photon Signatures for color octet at the LHC (and beyond)*, *J. High Energy Phys.* **05** (2020) 027, [[arXiv:2002.01474](#)].
- [16] C. T. Preuss and G. Valencia, *Long-lived electroweak-singlet colored scalars*, *Phys. Rev. D* **104** (2021), no. 9 095030, [[arXiv:2109.01261](#)].
- [17] A. Hayreter and G. Valencia, *Color-octet scalar decays to a gluon and an electroweak gauge boson in the Manohar-Wise model*, *Phys. Rev. D* **102** (2020), no. 11 115033, [[arXiv:1810.04048](#)].
- [18] L. M. Carpenter and S. Mantry, *Color-Octet, Electroweak-Doublet Scalars and the CDF Dijet Anomaly*, *Phys. Lett. B* **703** (2011) 479–485, [[arXiv:1104.5528](#)].
- [19] A. Hayreter and G. Valencia, *LHC constraints on color octet scalars*, *Phys. Rev. D* **96** (2017), no. 3 035004, [[arXiv:1703.04164](#)].
- [20] H. Georgi and M. Machacek, *DOUBLY CHARGED HIGGS BOSONS*, *Nucl. Phys. B* **262** (1985) 463–477.
- [21] M. S. Chanowitz and M. Golden, *Higgs Boson Triplets With $M(W) = M(Z) \cos \theta \omega$* , *Phys. Lett. B* **165** (1985) 105–108.
- [22] J. F. Gunion, R. Vega, and J. Wudka, *Higgs triplets in the standard model*, *Phys. Rev. D* **42** (1990) 1673–1691.
- [23] J. F. Gunion, H. E. Haber, G. L. Kane, and S. Dawson, *The Higgs Hunter’s Guide*, vol. 80. 2000.
- [24] K. Benakli, M. D. Goodsell, and A.-K. Maier, *Generating mu and Bmu in models with Dirac Gauginos*, *Nucl. Phys. B* **851** (2011) 445–461, [[arXiv:1104.2695](#)].
- [25] L. M. Carpenter and J. Goodman, *New Calculations in Dirac Gaugino Models: Operators, Expansions, and Effects*, *JHEP* **07** (2015) 107, [[arXiv:1501.05653](#)].
- [26] L. M. Carpenter and M. J. Smylie, *Exploring the phenomenology of weak adjoint scalars in minimal R-symmetric models*, *JHEP* **02** (2022) 102, [[arXiv:2108.02795](#)].
- [27] R. Boughezal and F. Petriello, *Precise predictions for Higgs production in models with color-octet scalars*, *Nucl. Phys. B Proc. Suppl.* **205-206** (2010) 289–294, [[arXiv:1006.5773](#)].
- [28] J. Cao, P. Wan, J. M. Yang, and J. Zhu, *The SM extension with color-octet scalars: diphoton enhancement and global fit of LHC Higgs data*, *JHEP* **08** (2013) 009, [[arXiv:1303.2426](#)].
- [29] N. D. Christensen and C. Duhr, *FeynRules — Feynman rules made easy*, *Comput. Phys. Commun.* **180** (Sep, 2009) 1614–1641.
- [30] A. Alloul, N. D. Christensen, C. Degrande, C. Duhr, and B. Fuks, *FeynRules 2.0 — A complete toolbox for tree-level phenomenology*, *Comput. Phys. Commun.* **185** (Aug, 2014) 2250–2300.
- [31] C. Degrande, C. Duhr, B. Fuks, D. Grellscheid, O. Mattelaer, and T. Reiter, *UFO — The Universal FeynRules Output*, *Comput. Phys. Commun.* **183** (Jun, 2012) 1201–1214, [[arXiv:1108.2040](#)].
- [32] J. Alwall, R. Frederix, S. Frixione, V. Hirschi, F. Maltoni, O. Mattelaer, H. S. Shao, T. Stelzer, P. Torrielli, and M. Zaro, *The automated computation of tree-level and next-to-leading order differential cross sections, and their matching to parton shower simulations*, *JHEP* **07** (2014) 079, [[arXiv:1405.0301](#)].
- [33] T. Sjöstrand, S. Ask, J. R. Christiansen, R. Corke, N. Desai, P. Ilten, S. Mrenna, S. Prestel, C. O. Rasmussen, and P. Z. Skands, *An introduction to pythia 8.2*, *Comput. Phys. Commun.* **191** (Jun, 2015) 159–177.
- [34] J. de Favereau, C. Delaere, P. Demin, A. Giammanco, V. Lemaitre, A. Mertens, and M. Selvaggi, *Delphes 3: a modular framework for fast simulation of a generic collider experiment*, *J. High Energy Phys.* **02** (Feb, 2014).
- [35] E. Conte, B. Fuks, and G. Serret, *MADANALYSIS 5, a user-friendly framework for collider phenomenology*, *Comput. Phys. Commun.* **184** (Jan, 2013) 222–256.
- [36] B. Field, *Distinguishing scalar from pseudoscalar Higgs production at the CERN LHC*, *Phys. Rev. D* **66** (2002) 114007, [[hep-ph/0208262](#)].
- [37] L. M. Carpenter, T. Murphy, and M. J. Smylie, *Changing patterns in electroweak precision fits with new color-charged states: Oblique corrections and the W-boson mass*, *Phys. Rev. D* **106** (2022), no. 5 055005, [[arXiv:2204.08546](#)].
- [38] S. Coleman, *Fun with SU(3)*, in *Seminar on high-energy physics and elementary particles*, pp. 331–352, 1965.
- [39] R. Slansky, *Group Theory for Unified Model Building*, *Phys. Rept.* **79** (1981) 1–128.